

Cluster formation, standing waves, and stripe patterns in oscillatory active media with local and global coupling

M. Falcke and H. Engel

Institut für Theoretische Physik, Technische Universität Berlin, Rudower Chaussee 5, Haus 2.14, 12484 Berlin, Germany

M. Neufeld

Institut für Theoretische Physik und Synergetik, Universität Stuttgart, Pfaffenwaldring 57, 70550 Stuttgart, Germany

(Received 16 August 1994)

In recent years, the effect of global coupling on spatiotemporal pattern formation in oscillatory media has attracted considerable interest. For the complex Ginzburg-Landau equation, modified by a global coupling term, we derive a criterion for cluster formation and discuss standing wave solutions with an intrinsic wavelength in the Benjamin-Feir stable parameter range. We argue that clustering expresses the dominance of global coupling. In two-dimensional media the interplay between the standing wave instability and anisotropic diffusion may generate stripe patterns coupled to a spatially uniform oscillating mode. Then, by direct numerical simulation, we show that the globally coupled reconstruction model—proposed by Krischer, Eiswirth, and Ertl for CO oxidation on Pt(110) [Surf. Sci. **900**, 251 (1991)]—exhibits clustering and predicts the presence of standing waves with an intrinsic wavelength.

PACS number(s): 82.20.Wt, 82.20.Mj, 82.65.Jv

I. INTRODUCTION

Currently, there is a growing interest in spatiotemporal patterns emerging as a result of global coupling in oscillatory active media [1–5]. In this paper we use two different approaches to investigate this problem. Our first model is the complex Ginzburg-Landau equation (CGLE) proposed by Mertens, Imbuhl, and Mikhailov [4],

$$\dot{\eta} = (1 - i\omega)\eta - (1 + i\beta)|\eta|^2\eta + (1 + i\varepsilon)\Delta\eta - \mu e^{i\chi}\bar{\eta}. \quad (1)$$

To account for global coupling, contrary to the usual form of the CGLE, Eq. (1) is modified by the additional last term, where

$$\bar{\eta} = \frac{1}{S} \int_S dz \eta(z, t) \quad (2)$$

denotes the spatial average of the complex oscillation amplitude. In Eq. (1) μ describes the strength of global coupling, χ is the phase shift between the driving force and the average complex amplitude, S denotes the system size, and z the spatial coordinate. Analyzing the stability of the homogeneous oscillatory solution of Eq. (1) we will derive a criterion for the formation of cluster states. We will show that this criterion coincides with an equivalent condition found recently by Hakim and Rappel's [3] con-

siderations of an ensemble of N identical, globally coupled Ginzburg-Landau oscillators without local coupling. Looking for modulated standing wave solutions of Eq. (1) we derive a set of coupled amplitude equations. By direct numerical simulation we demonstrate the existence of standing wave patterns and stripe-like oscillating patterns caused by anisotropic local coupling.

The second model starts from a kinetic scheme that has been proposed by Krischer, Eiswirth, and Ertl which describes kinetic oscillations during CO oxidation on platinum crystal surfaces under ultrahigh vacuum conditions [6]. Under experimental conditions corresponding to the oscillatory regime of the reaction, high-resolution measurements, obtained by photoemission electron microscopy, revealed unusual coverage patterns such as standing waves with an intrinsic wavelength, stripe patterns on an oscillating background, and turbulent patterns [7–9]. These spatiotemporal structures were associated with global coupling in the system whose existence has shown up in variations of the CO partial pressure in the gas phase, as verified experimentally [10]. Therefore, we add spatial coupling terms, one due to surface diffusion of adsorbed CO and the other to global coupling through the gas phase, to the kinetic scheme of Krischer, Eiswirth, and Ertl. Then we end with the following system of equations:

$$\frac{\partial c}{\partial t} = D \frac{\partial^2 c}{\partial z^2} + k_1 p_{\text{CO}} s_c \left[1 - \left(\frac{c}{c_s} \right)^3 \right] - k_2 c - k_3 c o, \quad (3)$$

$$\frac{\partial o}{\partial t} = k_4 p_{\text{O}_2} [(s_{\text{O}_1} - s_{\text{O}_2}) w + s_{\text{O}_2}] \left[1 - \frac{c}{c_s} - \frac{o}{o_s} \right]^2 - k_3 c o, \quad (4)$$

$$\frac{\partial w}{\partial t} = k_5 \begin{cases} -w, & 0.0 \leq \frac{c}{c_s} < 0.2 \\ -w - \frac{\left(\frac{c}{c_s}\right)^3 - 1.05 \left(\frac{c}{c_s}\right)^2 + 0.3 \frac{c}{c_s} - 0.026}{0.0135}, & 0.2 \leq \frac{c}{c_s} \leq 0.5 \\ -w + 1, & 0.5 < \frac{c}{c_s} \leq 1.0 \end{cases} \quad (5)$$

$$= k_5 \left[f \left[\frac{c}{c_s} \right] - w \right], \quad (5)$$

$$\frac{dp_{\text{CO}}}{dt} = \frac{J_{i0}}{V} \left\{ p_{\text{COE}} - p_{\text{CO}} \left[1 + \frac{V_{\text{ML}}}{J_{i0}A} \int_A dz^2 \left\{ k_1 p_{\text{CO}} \left[1 - \frac{c}{c_s} \right]^3 - k_2 \frac{c}{c_s} \right\} \right] \right\}. \quad (6)$$

Equation (3) for the coverage of carbon monoxide (c) describes adsorption and desorption of CO, as well as the formation of CO₂ according to a Langmuir-Hinshelwood mechanism. Local coupling on the surface is provided by the diffusion of adsorbed CO. The balance of oxygen coverage [o, Eq. (4)] includes the adsorption and reaction terms; contributions due to desorption and to diffusion of adsorbed oxygen may be ignored in the parameter range we are considering in the following. The kinetic scheme involves an adsorbate-driven phase transition of the Pt(110) surface between a 1×2 and a 1×1 structure. This is described by Eq. (5), where w denotes the fraction of the surface with a 1×1 structure, $1-w$ being the surface fraction with a 1×2 structure. The last equation, (6), for

the partial pressure of CO in the gas phase, has been obtained from the ideal gas law. It considers the volume current J_{i0} into (respectively, out of) the reactor and contributions due to adsorption and desorption of CO, where the corresponding terms have to be integrated over the whole surface (A). V_{ML} denotes the volume of one monolayer adsorbed CO in the reactor of volume V . For convenience, all parameters of the model are listed in Table I with their meaning and their numerical value defined for the following text. This table is taken from Ref. [6]. The numerical simulations carried out for the model (3)–(6) focus on the ability of the system to exhibit cluster formation and to support modulated standing waves with an intrinsic wavelength.

TABLE I. Parameters and variables of the reconstruction model.

Variables			
c	CO coverage		
o	O coverage		
w	Ratio of the surface in the 1×1 structure		
p_{CO}	Partial pressure of CO in the gas phase		
Parameters			
CO	k_1	Adsorption rate	$4.18 \times 10^5 \text{ MLs}^{-1} \text{ Torr}^{-1}$
	s_c	Sticking coefficient	1
	c_s	Saturation coverage	1 ML
O ₂	k_4	Adsorption rate	$7.81 \times 10^5 \text{ MLs}^{-1} \text{ Torr}^{-1}$
	s_{01}	Sticking coefficient on 1×1	0.6
	s_{02}	Sticking coefficient on 1×2	0.4
	o_s	Saturation coverage	0.8 ML
	p_{O_2}	Partial pressure of oxygen	
Rates with $k_i = A_i \exp(-E_i/RT)$, $i=1,2,3$			
	k_3	Reaction	$A_3 = 3 \times 10^6 \text{ (MLs)}^{-1}$ $E_3 = 10 \text{ kcal/mol}$
	k_2	CO desorption	$A_2 = 2 \times 10^{16} \text{ s}^{-1}$ $E_2 = 38 \text{ kcal/mol}$
	k_5	Phase transition	$A_5 = 200 \text{ s}^{-1}$ $E_5 = 7 \text{ kcal/mol}$
Local coupling			
	Diffusion coefficient $D = 10 \mu\text{m}^2\text{s}^{-1}$		
Global coupling			
	V	Volume of the reactor	55 l
	J_{i0}	Volume current into the reactor	360 l/s
	A	Crystal surface	
	V_{ML}	Volume of one monolayer adsorbed CO	
	p_{COE}	Partial pressure of CO in the gas inlet	

II. CLUSTERING IN DISTRIBUTED OSCILLATORY MEDIA WITH GLOBAL COUPLING

Equation (1) admits solutions in the form of uniform oscillations

$$\eta(x, t) = Ae^{i\Omega t}, \quad (7)$$

with amplitude A and frequency Ω according to

$$A^2 = 1 - \mu \cos \chi > 0, \quad \Omega = -\omega - \beta - \mu(\sin \chi - \beta \cos \chi). \quad (8)$$

In analyzing the stability of the uniform oscillatory state with respect to small perturbations $\rho \sim e^{i(kz + \Omega t) + \lambda t}$ of wave vector k , it must be noted that for nonuniform perturbations with $k \neq 0$ the average complex amplitude $\bar{\eta}$ vanishes, and we have to carry out the stability analysis for uniform and for nonuniform perturbations separately. Let us denote the growth rate of uniform perturbations by $\lambda(k=0)$. We emphasize that $\lambda(k=0)$ is different from $\lambda(k \rightarrow 0)$, the latter being the long wavelength limit of the growth rate of nonuniform perturbations. In the case where $k \neq 0$ we obtain the dispersion relation

$$\begin{aligned} \lambda(k) = & -k^2 + 2\mu \cos \chi - 1 \\ & \pm \{ -[\beta - \mu(\sin \chi + \beta \cos \chi) + \varepsilon k^2]^2 \\ & + (1 + \beta^2)(1 - \mu \cos \chi)^2 \}^{1/2}. \end{aligned} \quad (9)$$

Thus, in the limit $k \rightarrow 0$ the uniform oscillatory state becomes unstable if

$$2\mu \cos \chi - 1 > 0, \quad (10)$$

or when condition (10) does not hold, if

$$\mu[2 + \cos 2\chi + \beta \sin 2\chi] - 2(\cos \chi + \beta \sin \chi) < 0. \quad (11)$$

The last two conditions show how the Benjamin-Feir instability will be affected by the presence of global coupling. In the parameter range where (10) and (11) are satisfied the dispersion relation (9) has a shape, as shown in Fig. 1. The homogeneous oscillation is stable with respect to uniform perturbations [$\text{Re}\lambda(k=0) < 0$], but

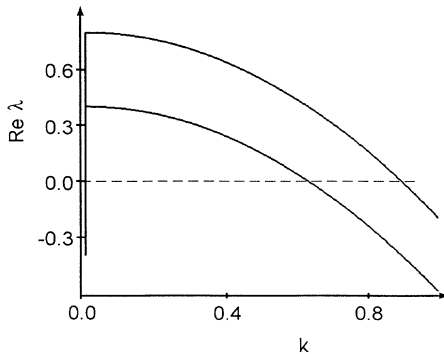


FIG. 1. Dispersion relation typical for the parameter range where clustering occurs. With respect to uniform perturbations the system is stable, corresponding to a peak downward in $\text{Re}\lambda$ at $k=0$.

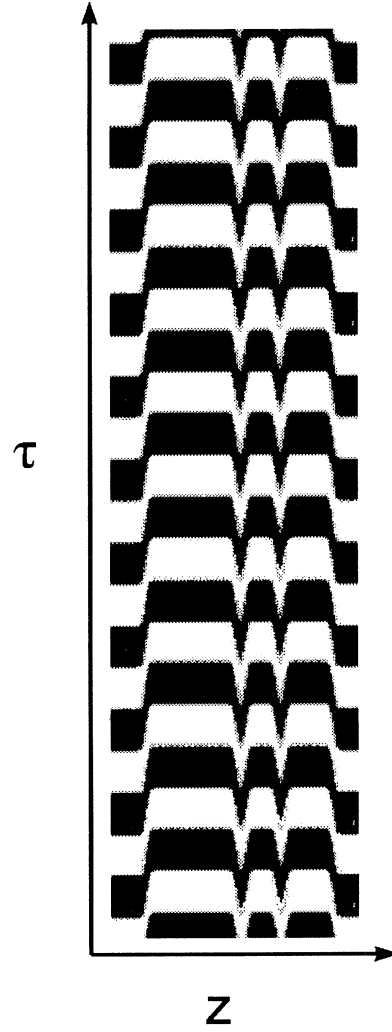


FIG. 2. Space time plot of a cluster pattern obtained with $\beta = -1.8$, $\omega = 0$, $\varepsilon = 0$, $\chi = 4.21$, and $\mu = 9.0$. In the notation of Hakim *et al.* these parameters are equivalent to $\mu' = 1.44$ and $\varepsilon' = -\beta' = 1.8$. Bright areas correspond to high values of $\text{Re}\eta$; dark areas to low values of $\text{Re}\eta$. τ and z denote the dimensionless time and spatial coordinate, respectively. In dimensionless units the system length is equal to 80.42 and the temporal period is 0.46.

unstable with respect to nonuniform perturbations with small k [$\text{Re}\lambda(k \rightarrow 0) > 0$]. In this situation the system exhibits clustering. The two clusters consist of local oscillators that have the same complex amplitude, but it differs from one cluster to the other cluster. In the distributed medium each cluster consists of one or a few synchronously oscillating spatial domains, as shown in Fig. 2.

For globally coupled Ginzburg-Landau oscillators without local coupling the phenomenon of cluster formation has been investigated by Hakim *et al.* using the system of equations

$$\begin{aligned} \eta'_j = & \mu' \eta'_j - (1 + i\beta') |\eta'_j|^2 \eta'_j + \frac{(1 + i\varepsilon')}{N} \sum_{i=1}^N (\eta'_i - \eta'_j), \\ & j = 1, \dots, N. \end{aligned} \quad (12)$$

For clustering the condition,

$$2\mu'(1+\beta'\varepsilon')+1+\beta'^2=0 \quad (13)$$

has been derived. We will now show that both criteria, i.e., (10), (11), and (13), coincide. Applying the transformation

$$\begin{aligned} \eta &= [\mu \cos(\chi + \pi)]^{1/2} e^{i[\omega - \mu \sin(\chi + \pi)]\tau} \eta', \\ \tau &= \frac{\tau'}{\mu \cos(\chi + \pi)}, \\ \mu' &= \frac{1 + \mu \cos(\chi + \pi)}{\mu \cos(\chi + \pi)}, \\ \beta &= \beta', \\ \varepsilon' &= \tan \chi \end{aligned} \quad (14)$$

to Eq. (1) we obtain Hakim's equation (12). The real part of the prefactor in the coupling term of Eq. (12) is positive. According to that we require $\pi/2 < \chi < 3\pi/2$ in Eq. (1). This implies that $\mu' > 0$ and $2\mu \cos \chi - 1 < 0$, i.e., condition (10) is not satisfied. Under the transformation (14) from the second condition, Eq. (11) follows Eq. (13). We conclude that the threshold for clustering is the same for oscillators exclusively coupled globally, Eq. (12), and for the distributed oscillatory medium described by Eqs. (1) and (2), where global and local coupling act simultaneously.

In the parameter space next to the region with cluster formation Hakim finds a region with chaotic behavior. For adequate parameter values that are determined according to (14), we observe this transition with Eq. (1) in the distributed medium, too. We argue that global coupling governs the behavior of the system not only close to

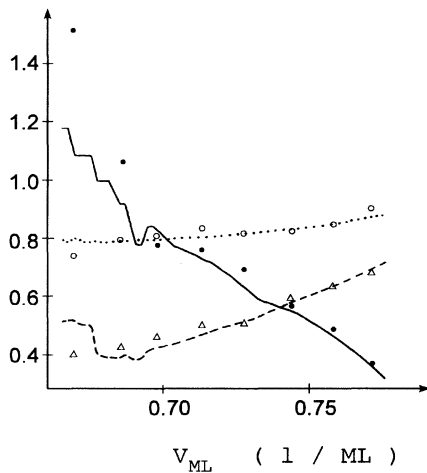


FIG. 3. Main characteristic features of clusters in dependence of V_{ML} . The lines show the results obtained for oscillators coupled only globally and the symbols the results for both locally and globally coupled oscillators, respectively: size ratio, solid line and dots; amplitude ratio, dashed line and triangles; phase shift, dotted line and open circles. The parameters are $p_{O_2} = 1.17 \times 10^{-4}$ Torr, $p_{CO_2} = 4.0 \times 10^{-5}$ Torr, $T = 545$ K, $J_{10} = 360$ l/s, $V = 55$ l. V_{ML} is in units of $1/ML$ (ML , monolayer).

the onset of cluster formation but in a whole parameter region that extends at least up to the mentioned transition to chaotic motion. Here, clustering expresses the dominance of global over local coupling in distributed oscillatory media.

Next, we turn to consider the reconstruction model, Eqs. (3)–(6). In this case we have determined the dispersion relation numerically. In a certain parameter range the Floquet exponent L —representing stability of the uniform oscillatory state with respect to nonuniform perturbations—may become positive [11]. This parameter range does not depend on whether local coupling was taken into account ($D \neq 0$) or not ($D = 0$). Inside this parameter range the homogeneous oscillation decomposes into a two-cluster solution. The characteristic features of the cluster solution are the size ratio, the amplitude ratio, and the phase shift between the clusters. In Fig. 3 these quantities are plotted against the global coupling parameter V_{ML} , both with and without local coupling in the system. The deviations between the two cases are small except for low V_{ML} values, whether the clusters exhibit irregular oscillations without local coupling. Thus the numerical results support the point of view that there exists a whole parameter range where pattern formation in Eqs. (3)–(6) is governed by global coupling. In the next section we discuss the standing waves created due to the presence of global coupling.

III. MODULATED STANDING WAVES WITH AN INTRINSIC WAVELENGTH

We start with the CGLE and consider the Benjamin-Feir stable case $1 + \varepsilon\beta > 0$, looking for standing waves generated by global coupling. By numerical simulation of the globally coupled CGLE [Eqs. (1) and (2)] we found standing waves with an intrinsic wavelength provided the growth rate λ has a positive global maximum at k_{max} ,

$$k_{max}^2 = -\frac{1}{\varepsilon} \left[\beta - \mu(\sin \chi + \beta \cos \chi) + \left[\frac{1 + \beta^2}{1 + \varepsilon^2} (1 - \mu \cos \chi)^2 \right]^{1/2} \right] \quad (15)$$

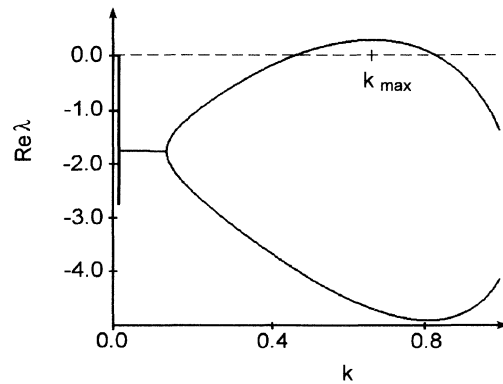


FIG. 4. Dispersion relation for $\beta = 1.56$, $\omega = 0$, $\varepsilon = 4.8$, $\chi = 1.65$, $\mu = 4.8$. k_{max} obeys Eq. (15).

at a finite distance from zero (compare Fig. 4), and if the global coupling is destabilizing, i.e., $\pi/2 < \chi < 3\pi/2$. For stabilizing global coupling, $-\pi/2 < \chi < \pi/2$, standing waves were found only as a transient pattern.

Now we ask for modulated standing wave solutions of Eqs. (1) and (2) in the form

$$\eta(\tau, z) = \eta_0(\tau) + \eta_k(\tau)(e^{ikz} + e^{-ikz}). \quad (16)$$

η_0 represents the spatially uniform mode and η_k the amplitude of the standing wave. The ansatz (16) is supported by the Fourier analysis of the simulation data that revealed that about 85% of the spectral power is concentrated in the first order spatial mode. In the following we restrict ourselves to the parameter range where the approximation (16) is meaningful and after substituting it into (1), all spatial modes of higher order may be neglected. Then we find the following coupling equations for the amplitudes η_0 and η_k :

$$\begin{aligned} \dot{\eta}_0 &= (1 - i\omega - \mu e^{i\chi})\eta_0 - (1 + i\beta)|\eta_0|^2\eta_0 \\ &\quad - 4(1 + i\beta)|\eta_k|^2\eta_0 - 2(1 + i\beta)\eta_k^2\eta_0^*, \\ \dot{\eta}_k &= [1 - i\omega - (1 + i\epsilon)k^2]\eta_k - 3(1 + i\beta)|\eta_k|^2\eta_k \\ &\quad - 2(1 + i\beta)|\eta_0|^2\eta_k - 2(1 + i\beta)\eta_0^2\eta_k^*. \end{aligned} \quad (17)$$

We assume the following time dependence for η_0 and η_k :

$$\eta_0 = E_0 e^{-i(\omega + \Omega)\tau}, \quad \eta_k = E_k e^{-i[(\omega + \Omega)\tau + \gamma]}. \quad (18)$$

For the amplitudes E_0 and E_k , the frequency Ω , and the phase shift γ , we find with (17) the equations

$$\begin{aligned} 1 + i\Omega - \mu e^{i\chi} &= (1 + i\beta)E_0^2 + 2(1 + i\beta)(2 + e^{2i\gamma})E_k^2, \\ 1 + i\Omega - (1 + i\epsilon)k^2 &= 3(1 + i\beta)E_k^2 \\ &\quad + 2(1 + i\beta)(2 + e^{2i\gamma})E_0^2. \end{aligned} \quad (19)$$

The solution of (19) reads

$$\begin{aligned} E_k^2 &= \frac{1 - k^2 - 2(1 - \mu \cos \chi)(1 + \cos 2\gamma + \beta \sin 2\gamma)}{3 - 4(1 + \cos 2\gamma + \beta \sin 2\gamma)(2 + \cos 2\gamma - \beta \sin 2\gamma)}, \\ E_0^2 &= \frac{3(1 - \mu \cos \chi) - 2(1 - k^2)(2 + \cos 2\gamma - \beta \sin 2\gamma)}{3 - 4(1 + \cos 2\gamma + \beta \sin 2\gamma)(2 + \cos 2\gamma - \beta \sin 2\gamma)}, \\ \Omega &= \beta - (\beta - \epsilon)k^2 - 2(1 + \beta^2)\sin 2\gamma \frac{3(1 - \mu \cos \chi) - 2(1 - k^2)(2 + \cos 2\gamma - \beta \sin 2\gamma)}{3 - 4(1 + \cos 2\gamma + \beta \sin 2\gamma)(2 + \cos 2\gamma - \beta \sin 2\gamma)}, \end{aligned} \quad (20)$$

where γ has to be determined from the following fourth order algebraic equation for $\tan \gamma$:

$$\begin{aligned} \sum_{i=0}^4 r_i \tan^i \gamma &= 0, \quad \text{with} \\ r_0 &= 21[(\beta - \epsilon)k^2 + \mu(1 + \beta^2)^{1/2} \sin(\chi - \chi')] = -7r_4, \\ r_1 &= 4[(1 + \beta^2)(6 - 3k^2 - \mu \cos \chi) - 2(1 + \beta\epsilon)k^2 \\ &\quad + 2\mu\beta(1 + \beta^2)^{1/2} \sin(\chi - \chi')], \\ r_2 &= 16\beta[(1 + \beta\epsilon)k^2 - \mu(1 + \beta^2)^{1/2} \cos(\chi + \chi')] \\ &\quad + 2[(\beta - \epsilon)k^2 + \mu(1 + \beta^2)^{1/2} \sin(\chi - \chi')], \\ r_3 &= 4[(1 + \beta^2)(k^2 + \mu \cos \chi - 2) - 2(1 + \beta\epsilon)k^2 \\ &\quad + 2\mu(1 + \beta^2)^{1/2} \cos(\chi + \chi')]. \end{aligned} \quad (21)$$

Here $\tan \chi' = \beta$. Because $r_0 = -7r_4$ Eq. (21) possesses at least two real solutions for $\tan \gamma$. To compare the analytical and the numerical results we have taken, for example, the parameter values $\epsilon = 8$, $\beta = 1.4$, $\chi = 1.65$, $\mu = 6$, and $k = k_{\max} = 0.6710$. Then, from (20) and (21) we get $E_0 = 0.7525$, $E_k = 0.3507$, $\Omega = 7.3862$, and $\gamma = -0.5649$. From numerical simulations we obtain $E_0 = 1.0978$, $E_k = 0.3036$, and $\Omega = 7.9467$. If we use the wave vector $k = 0.6749$, which was found numerically, instead of k_{\max} , then we have $E_0 = 0.7461$, $E_k = 0.3526$, $\Omega = 7.3762$, and $\gamma = -0.5672$. Bearing in mind that higher order spatial modes contribute about 15% to the spatial ampli-

tude of the standing wave, the agreement is satisfactory.

Figure 5 summarizes the qualitative changes in the shape of the dispersion relation that occurs under variation of the parameters ϵ and μ , characterizing the strength of local and global coupling, respectively. The broken line marks the locus of the Benjamin-Feir instability given by $1 + \epsilon\beta = 0$. Typical spatiotemporal patterns associated with different regions in the parameter plane are cluster formation and oscillating domains (region a); cluster states modified by a periodic spatial structure (region b); standing waves with an intrinsic wavelength (region c); and homogeneous oscillations (region d). This sequence of transitions (a–d) occurs when increasing μ , provided ϵ exceeds some β - and χ -dependent threshold. The change in the curvature of the dispersion relation at $k = 0$ defines the boundary between simple cluster patterns (compare Fig. 2) and cluster patterns modified by a periodic spatial structure. The behavior in the Benjamin-Feir unstable parameter region, denoted in Fig. 5, was studied by Mertens, Imbihl, and Mikhailov [12].

The standing waves change their properties inside region (c) of Fig. 5. Sufficiently far away from line 1, when $\text{Re}\lambda(k \rightarrow 0) \ll 0$, modulated standing waves with constant in space amplitude appear as shown in Fig. 6. Their wavelength is in the unstable k range in the vicinity of k_{\max} . The intrinsic character of the wavelength has been verified numerically for random initial conditions: no influence of the system size or the boundary conditions has been observed. If $\text{Re}\lambda(k \rightarrow 0)$ becomes close to zero,

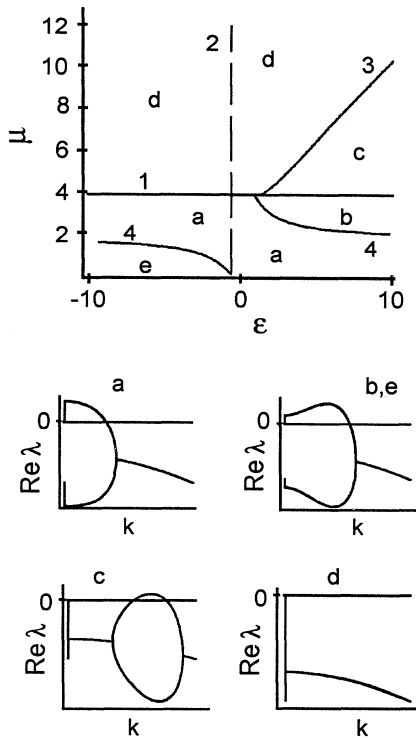


FIG. 5. Regimes of behavior of an oscillatory medium described by the globally coupled CGLE in the μ - ϵ parameter plane for $\beta=1.56$ and $\chi=1.65$. Lines 1 to 3 are defined from the following conditions: 1- $\text{Re}\lambda(k \rightarrow 0)=0$, 2-Benjamin-Feir line $1 + \epsilon\beta=0$, 3- $\text{Re}\lambda(k_{\max})=0$, and 4- $d^2\text{Re}\lambda(k)/dk^2|_{k=0}=0$. The shape of the dispersion relation in parameter region a-e is shown, too. Key: a, cluster states; b,e, cluster states modified by a periodic spatial structure; c, standing waves; and d, homogeneously oscillating state.

clustering as well as spatial modes influence the pattern. It becomes obvious if we compare this with the situation without local coupling, when $\text{Re}\lambda(k \rightarrow 0)$ is positive, but close to zero. Then the size of the two clusters may be significantly different. The smaller cluster oscillates with the larger amplitude. This is reflected also in the one dimensional pattern shown in Fig. 7. There is a broad spatial range oscillating with small temporal and spatial amplitudes and a smaller range with large temporal and spatial amplitudes.

Standing waves exist only beyond critical values μ_{cr} and ϵ_{cr} . In Fig. 8 μ_{cr} has been determined from the condition $\text{Re}\lambda(k \rightarrow 0)=0$; for $\mu > \mu_{\text{cr}}$ we have $\text{Re}\lambda(k \rightarrow 0) < 0$. The value of ϵ_{cr} follows from the condition $\text{Re}\lambda(k_{\max})=0$ with $\text{Re}\lambda(k_{\max}) > 0$ for $\epsilon > \epsilon_{\text{cr}}$.

Besides the described modulated standing waves in the same parameter range another pattern with a wave vector $k = 2\pi/S$ as the basic mode was found. This wave pattern arises only from near symmetrical initial conditions. Both patterns correspond to different values of the average complex amplitude $\bar{\eta}$. The $\bar{\eta}$ value associated with the modulated standing waves is about ten times larger than that of the pattern with the size-dependent wavelength.

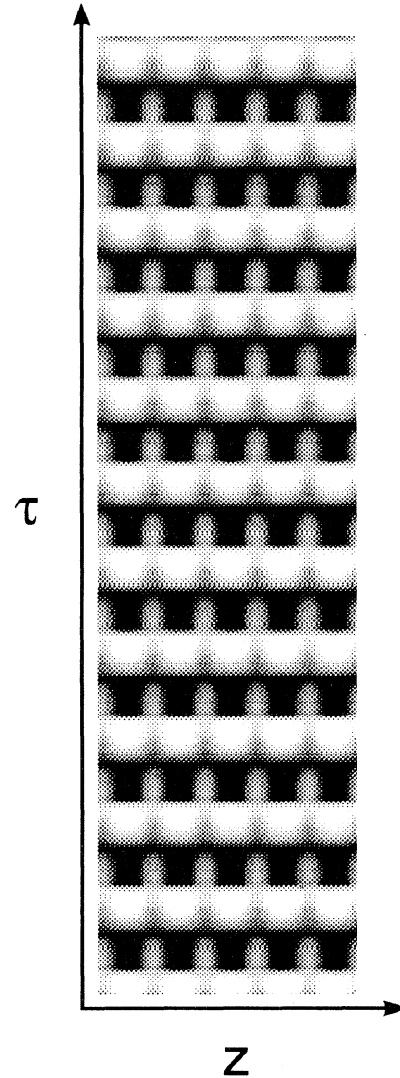


FIG. 6. Space time plot of a standing wave obtained for $\beta = -1.5$, $\omega = 0$, $\epsilon = -5$, $\chi = 4.587$, $\mu = 4.0$. τ and z denote the dimensionless time and spatial coordinate, respectively. The system length is equal to 50.26.

Returning once more to the reconstruction model with global coupling Eqs. (3)–(6), we find within this model standing wave patterns with an intrinsic wavelength located in two different parameter ranges. In the first range for the Floquet exponents of the uniform oscillatory state we have the conditions $\text{Re}L(k \rightarrow 0) > 0$ and $\text{Re}L(k_{\max}) > \text{Re}L(k \rightarrow 0)$. As shown in Fig. 9, here cluster states modulated by a shorter standing wave occur similarly to those observed with the CGLE near the boundary $\text{Re}\lambda(k \rightarrow 0)=0$. The parameter range in the $P_{\text{COE}}-P_{\text{O2}}$ plane, where for any V_{ML} a dispersion relation with the indicated properties exists, is plotted in Fig. 10.

The second parameter range with standing waves is located between the parameters for which clustering occurs and the parameters corresponding to turbulent patterns.

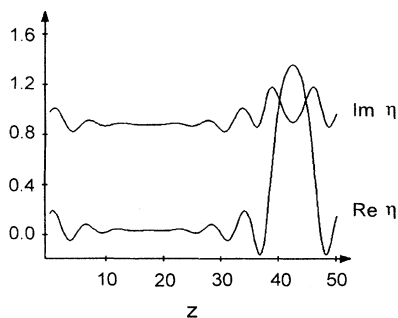


FIG. 7. Modulated cluster pattern influenced by spatial modes with $k \leq k_{\max}$ for $\epsilon = -2$, $\beta = -1.7$, $\omega = 0$, $\chi = 4.6338$, and $\mu = 4.1$. Then without local coupling the size ratio of the two clusters is equal to 11.5. In the distributed medium this results in the formation of a broad spatial domain with small temporal and spatial amplitudes and a comparably narrow region with large spatial amplitudes. z denotes the dimensionless spatial coordinate. The system length is equal to 50.26, and the temporal period is 1.14 in dimensionless units.

Here the homogeneous state is stable. Nevertheless, modulated standing waves were obtained as shown in the space-time plot on Fig. 11. We observe a certain range of allowed wavelengths that become slightly shorter with decreasing V_{ML} . Figure 12 shows the wavelength as a function of the system size S . On the upper branch the system contains three wavelengths, and on the lower one, four wavelengths. The wavelength difference between the two branches provides a rough estimate for the width of the stable band. In the range where the two branches overlap, the patterns corresponding to the upper branch exhibit strong amplitude oscillations. Outside this coexistence range the wavelength is independent of the initial condition. For periodic initial conditions with a wavelength below the wavelength band, the system reaches the homogeneous oscillatory state, occasionally after a very long transient. If the wavelength of the initial condition

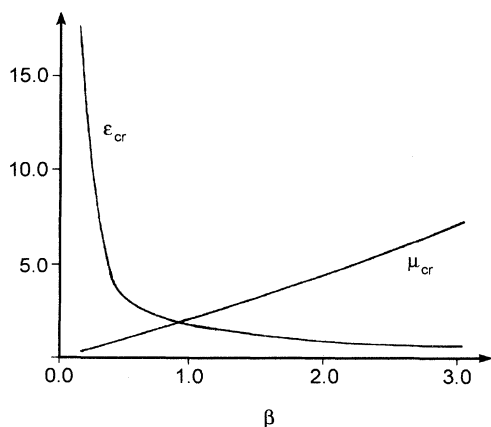


FIG. 8. Critical values for the onset of the standing wave instability, ϵ_{cr} and μ_{cr} , as a function of β for $\chi = 1.65$.

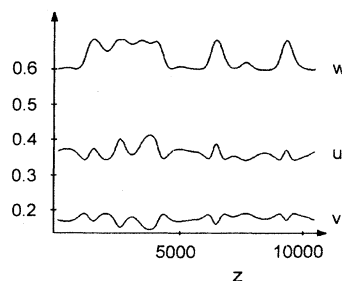


FIG. 9. Modulated cluster pattern obtained with the globally coupled reconstruction model for $p_{\text{O}_2} = 1.68 \times 10^{-4}$ Torr, $p_{\text{COE}} = 4.734 \times 10^{-5}$ Torr, $T = 545$ K, $V_{\text{ML}} = 0.095$ l/ML, $J_{i0} = 360$ l/s, $V = 55$ l, and $k_5 = 400$ s $^{-1}$. u denotes the CO coverage, v the O coverage, and w the fraction of the surface with the 1×1 structure. z is the spatial coordinate in dimensionless units. The length of the system is 2.171 mm. The temporal period is 2.45 s.

is higher than the band, then the system turns into the modulated standing wave. The wavelength is independent of the boundary conditions (see Fig. 12).

IV. STRIPE PATTERNS DUE TO ANISOTROPIC DIFFUSION

Among the spatiotemporal patterns observed in experimental studies of CO oxidation on Pt(110) stripelike patterns has been observed. We argue that stripes may be generated if the standing wave instability takes place in a medium with anisotropic diffusion. For CO oxidation on Pt(110) the adsorbate-induced phase transition leads to an anisotropy of the crystal surface with respect to diffusion of adsorbed CO. The diffusion is increased by a factor of up to 10 in the [110] compared with the diffusion in the [001] crystallographic direction.

To test our idea, we have carried out two-dimensional simulations with the CGLE [Eqs. (1) and (2)] using

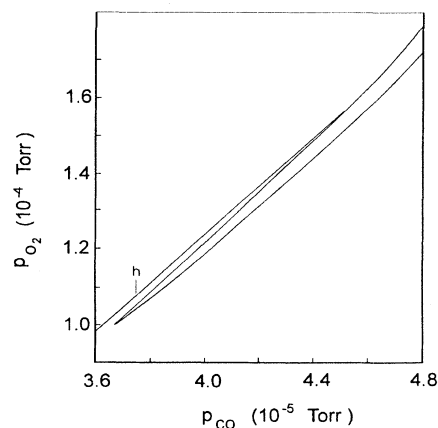


FIG. 10. Parameter range in the $p_{\text{COE}}-p_{\text{O}_2}$ plane, where for any V_{ML} dispersion relations with the properties $\text{Re}\lambda(k \rightarrow 0) > 0$ and $\text{Re}\lambda(k_{\max}) > \text{Re}\lambda(k \rightarrow 0)$ exists; $T = 54$ K, $J_{i0} = 360$ l/s, and $V = 55$ l.

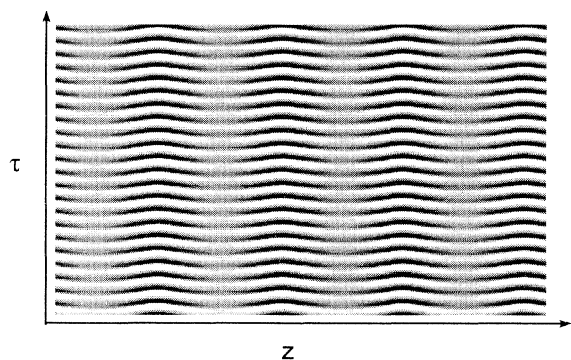


FIG. 11. Space time plot of a standing wave at $p_{O_2}=1.16 \times 10^{-4}$ Torr, $p_{COE}=4.0 \times 10^{-5}$ Torr, $T=545$ K, $V_{ML}=0.75$ l/ML, $J_{i0}=360$ l/s, $V=55$ l. Bright (dark) grey level represents an area with high (low) CO coverage. τ and z denote the dimensionless time and spatial coordinate, respectively. The length of the system is 0.677 mm. The temporal period is 4.21 s.

different values for ϵ during the calculations: $\epsilon=0.96$ in one spatial direction, and $\epsilon=4.8$ in the other. For the chosen values of the remaining parameters in the CGLE with $\epsilon=0.96$, $\text{Re}\lambda(k)$ is negative for all k , whereas with $\epsilon=4.8$ the standing wave instability occurs. Figure 12 presents the result of the simulation. The stripes of the pattern are perpendicular to the direction with faster diffusion. Thus we conclude that the stripe pattern may be interpreted as the result of the standing wave instability under spatial anisotropic conditions. Note that the stripe pattern is stable with respect to topological defects. This also follows from Fig. 13, where a topological defect disappears in the course of time.

V. DISCUSSION

We study spatiotemporal structures that appear in oscillatory active media with global coupling between indi-

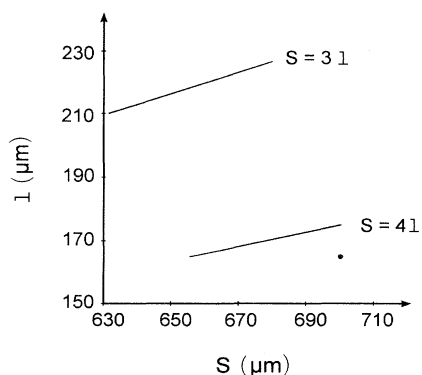


FIG. 12. Wavelength l of the standing wave obtained with the reconstruction model as a function of the system size S for $p_{O_2}=1.16 \times 10^{-4}$ Torr, $p_{COE}=4.0 \times 10^{-5}$ Torr, $T=545$ K, $V_{ML}=0.75$ l/ML, $J_{i0}=360$ l/s, and $V=55$ l. The lines are determined from periodic boundary conditions. The dot denotes a wavelength found using no flux boundary conditions.

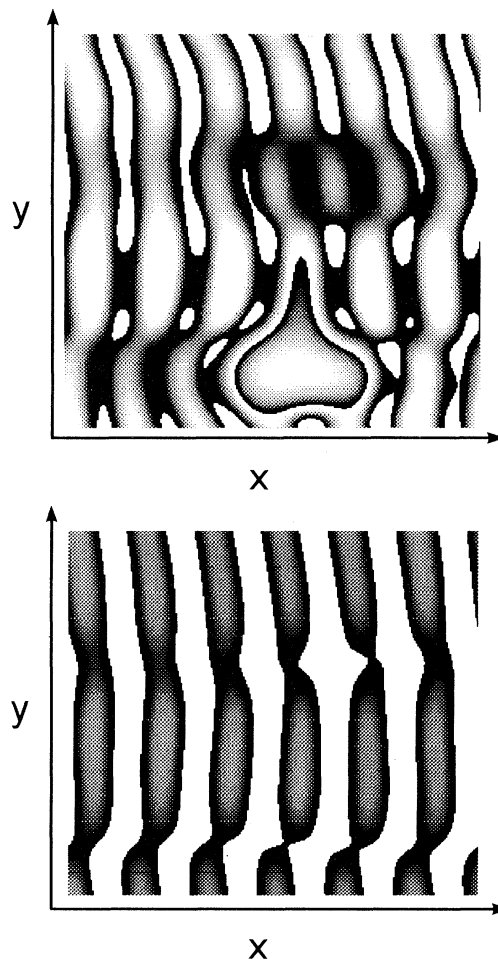


FIG. 13. Snapshots of a pattern showing $\text{Re}\eta$ at two different time moments, $\tau=77.5$ (top) and $\tau=102.8$ (bottom). The pattern was obtained by numerical solution of the globally coupled CGLE in two spatial dimensions for $\beta=1.56$, $\omega=0$, $\chi=1.65$, and $\mu=4.8$. To introduce an anisotropic local coupling, different values for ϵ have been chosen in the x and y direction: $\epsilon_x=4.8$ and $\epsilon_y=0.96$. Bright areas correspond to high values of $\text{Re}\eta$, dark areas to low values of $\text{Re}\eta$. The system size is 50.26×50.26 in dimensionless units.

vidual oscillators, alongside local coupling by diffusion. Our investigations are based on the CGLE and on the reconstruction model for the CO oxidation on Pt(110), both modified by terms describing global coupling. With both models we found that dominance of global coupling manifests itself in the formation of clusters. The clusters form synchronously oscillating spatial domains without an intrinsic characteristic length scale. There exists, however, a region in parameter space where global and local coupling jointly cooperate and the final pattern is a modulated standing wave with an intrinsic wavelength. For the CGLE the standing wave instability appears in the Benjamin-Feir stable case $1+\epsilon\beta>0$. It is induced by the global coupling and disappears if the coupling strength becomes small enough. In addition there should be a sufficiently high level of local coupling. For the

reconstruction model, standing waves with an intrinsic wavelength could also be observed. In one spatial dimension we have carried out extensive numerical simulations to prove that the wavelength is independent of initial and boundary conditions as well as of the system size.

The Ginzburg-Landau and reconstruction models differ with respect to the patterns coexisting with the standing wave solution. The standing wave pattern obtained with the reconstruction model coexists with the uniform oscillating state. In contrast to that, the standing wave pattern found with the CGLE model coexists with another standing wave, the wavelength of which is always equal to the system length S .

With the CGLE model in a parameter region where $\text{Re}\lambda(k_{\text{max}}) > \text{Re}\lambda(k \rightarrow 0) > 0$, spatially modulated clusters arise. In this regime a preferred wave vector can also be observed, but now it can be any value from the interval $0 < k < k_{\text{max}}$, i.e., k is not necessarily close to k_{max} . The reconstruction model also exhibits spatially modulated cluster solutions [13]. Mertens, Imbihl, and Mikhailov studied the CGLE [4,12] in the limit of small coupling strength $\mu \ll 1$. For sufficiently strong global coupling they found standing waves in the Benjamin-Feir unstable parameter range. In this case global coupling transforms an unstable phase-turbulent pattern into a standing wave pattern. In contrast to that, we have studied herein the Benjamin-Feir stable regime, where an instability to standing waves is induced by the global coupling.

Recently, Levine and Zou derived coupled CGLE models, valid near the Hopf bifurcation of the reconstruction model and modified by additional terms to ac-

count for global couplings [1,2]. Near a codimension-two point, where the global oscillation and spatial nonuniform modes with $q \neq 0$ simultaneously undergo a Hopf bifurcation with similar frequencies, this set of coupled amplitude equations predicts the presence of standing waves modulated by an overall global oscillation. These waves can be obtained even without global coupling, due to parametric resonance. The authors propose that they describe most closely the experimentally observed waves.

We remark that the standing wave patterns observed so far in experiments with the CO oxidation on Pt(110) surfaces differ in some respect from the standing wave solutions obtained in the reconstruction model, Eqs. (3)–(6). At a fixed moment in time the spatial profiles of the standing waves, viewed in the experiments, exhibit periodically spaced pronounced peaks. A half time period later the profile looks exactly the same, only shifted in space by half a wavelength. The standing wave solution of the reconstruction model shows pronounced peaks in the spatial profile, too. However, now a half time period later, the peaks form at the same position but they point downward, i.e., instead of a sharp local maximum, a sharp local minimum develops. Thus, unresolved questions still remain in the comprehension of the standing wave pattern in the CO oxidation on Pt(110).

ACKNOWLEDGMENTS

This work was supported by a grant from the Deutsche Forschungsgemeinschaft. We thank R. Friedrich for helpful discussions.

-
- [1] H. Levine and X. Zou, *Phys. Rev. Lett.* **69**, 204 (1992).
 - [2] H. Levine and X. Zou, *Phys. Rev. E* **48**, 50 (1994).
 - [3] V. Hakim and W.-J. Rappel, *Phys. Rev. A* **46**, R7347 (1992).
 - [4] F. Mertens, R. Imbihl, and A. Mikhailov, *J. Chem. Phys.* **99**, 8668 (1993).
 - [5] M. Falcke and H. Engel, *Phys. Rev. E* **50**, 1353 (1994).
 - [6] K. Krischer, M. Eiswirth, and G. Ertl, *Surf. Sci.* **900**, 251 (1991).
 - [7] S. Nettesheim, A. v. Oertzen, and G. Ertl, *J. Chem. Phys.* **98**, 9977 (1993).
 - [8] S. Jakubith, H. H. Rothermund, W. Engel, A. v. Oertzen, and G. Ertl, *Phys. Rev. Lett.* **65**, 3013 (1990).
 - [9] H. H. Rothermund, S. Jakubith, A. v. Oertzen, and G. Ertl, *Phys. Rev. Lett.* **66**, 3083 (1991).
 - [10] M. Eiswirth, P. Möller, K. Wetzl, R. Imbihl, and G. Ertl, *J. Chem. Phys.* **90**, 510 (1989).
 - [11] M. Falcke and H. Engel, *J. Chem. Phys.* **101**, (7) (1994).
 - [12] F. Mertens, R. Imbihl, and A. Mikhailov, *J. Chem. Phys.* **101**, 9903 (1994).
 - [13] M. Bär, M. Hildebrand, M. Eiswirth, M. Falcke, H. Engel, and M. Neufeld, *Chaos* **4**, 499 (1994).

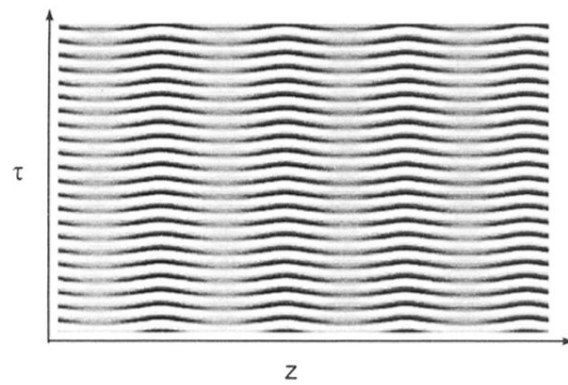


FIG. 11. Space time plot of a standing wave at $p_{\text{O}_2} = 1.16 \times 10^{-4}$ Torr, $p_{\text{COE}} = 4.0 \times 10^{-5}$ Torr, $T = 545$ K, $V_{\text{ML}} = 0.75$ l/ML, $J_{i0} = 360$ l/s, $V = 55$ l. Bright (dark) grey level represents an area with high (low) CO coverage. τ and z denote the dimensionless time and spatial coordinate, respectively. The length of the system is 0.677 mm. The temporal period is 4.21 s.

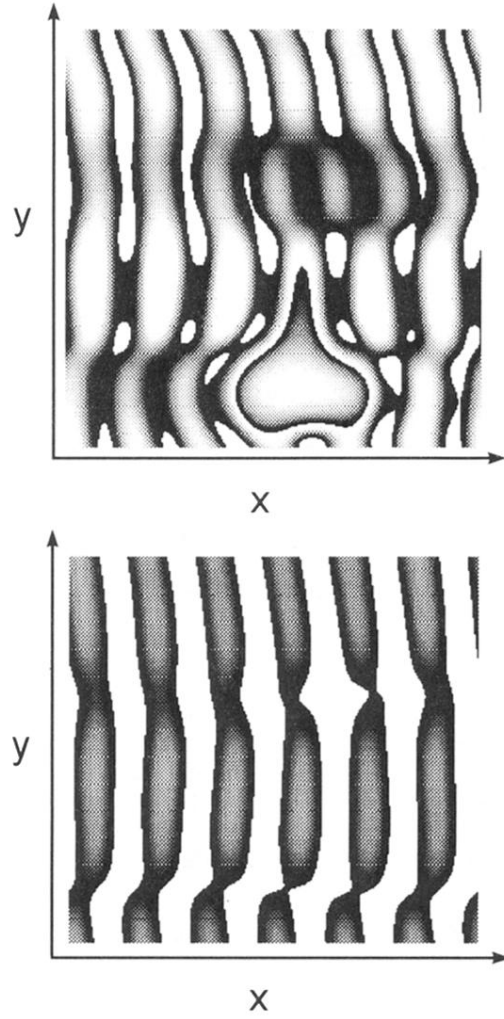


FIG. 13. Snapshots of a pattern showing $\text{Re}\eta$ at two different time moments, $\tau=77.5$ (top) and $\tau=102.8$ (bottom). The pattern was obtained by numerical solution of the globally coupled CGLE in two spatial dimensions for $\beta=1.56$, $\omega=0$, $\chi=1.65$, and $\mu=4.8$. To introduce an anisotropic local coupling, different values for ϵ have been chosen in the x and y direction: $\epsilon_x=4.8$ and $\epsilon_y=0.96$. Bright areas correspond to high values of $\text{Re}\eta$, dark areas to low values of $\text{Re}\eta$. The system size is 50.26×50.26 in dimensionless units.